

Biomass-Derived Stress-Regulating Additives for Microsilicon Anodes in Lithium-Ion Batteries

Luwen Li, Qitao Shi,* Zhipeng Wang, Cheng Zhang, Jiaqi Wang, Junjin Zhang, Xiangqi Liu, Alicja Bachmatiuk, Ruizhi Yang,* Yanbin Shen,* and Mark H. Rümmeli*

Microsilicon (μ Si) anode, with an ultrahigh capacity of 3579 mAh g^{-1} , presents less interfacial side reactions and lower production costs compared to nanosilicon, making it a promising candidate for lithium-ion batteries. However, the severe local stress produced upon repeated lithium insertion and extraction causes structural deterioration, significantly reducing the cycling stability of μ Si anodes. Here, biomass-derived carbon microtubes are introduced into μ Si electrodes as elasticity mediators to alleviate the stress generated during electrode cycling. After carbonization at a moderate temperature of 370°C , the carbon tube walls retain some organic ingredients and exhibit impressive

elasticity and resilience, which can effectively alleviate the volume expansion of μ Si particles and prevent pulverization of the electrode. In addition, the large inner diameter of the carbon tube provides additional space to compensate for the volume expansion of microsized silicon. The μ Si anode with carbon microtubes additives delivers an enhanced capacity of 1047 mAh g^{-1} after 200 cycles at a high current density of 2 A g^{-1} . These results indicate that carbon microtubes are efficient stress-regulating additives for μ Si anodes, and further research may extend their application to other high-capacity alloy anodes, such as SiO_x , phosphorus-based, and tin-based anodes.

1. Introduction

Lithium-ion batteries (LIBs) are widely used in applications such as electric vehicles and portable devices, which significantly facilitate our daily lives and promote sustainable development.^[1] As the demand for higher energy density in electric vehicles increases, exploring alternative anode materials to graphite is essential. In addition to natural abundance,^[2] silicon (Si) has high theoretical specific capacity (3579 mAh g^{-1})^[3] and a moderate voltage plateau. However, the huge volume expansion of Si particles during lithiation and delithiation causes severe particle pulverization, loss of electrical contact, and unstable solid-electrolyte interface (SEI) formation, further degrading the

Coulombic efficiency and resulting in limited cell cycle life.^[4] To solve this problem, researchers have explored the use of Si nanoparticles and wires.^[5] However, troublesome interfacial side reactions caused by the large specific surface area of nanoscale Si and its low tap density hinder its practical application.^[6] In contrast, microsilicon (μ Si) offers benefits such as fewer electrochemical side reactions and lower production costs when considered for practical use as an anode material in LIBs.^[7]

To address the issue of rapid electrode cracking owing to volume changes, various strategies have been proposed, including electrolyte modification,^[8] functional binder materials,^[9] novel electrode structure designs,^[10,6b] and the development of innovative conductive additives.^[11] The use of stress-regulating

L. Li, Z. Wang, C. Zhang, J. Wang, J. Zhang, X. Liu, R. Yang
College of Energy
Soochow Institute for Energy and Materials Innovation
Key Laboratory of Advanced Carbon Materials and Wearable Energy
Technologies of Jiangsu Province
Key Laboratory of Core Technology of High Specific Energy Battery and
Key Materials for Petroleum and Chemical Industry
Soochow University
Suzhou 215006, P. R. China
E-mail: yangrz@suda.edu.cn

Q. Shi, Y. Shen
I-Lab
CAS Center for Excellence in Nanoscience
Suzhou Institute of Nano-Tech and Nano-Bionics (SINANO)
Chinese Academy of Sciences (CAS)
Suzhou 215123, P. R. China
E-mail: qtshi2023@sinano.ac.cn
ybshen2017@sinano.ac.cn

A. Bachmatiuk
Faculty of Chemistry
Wrocław University of Science and Technology
Wybrzeże Wyspińskiego 27, 50-370 Wrocław, Poland

A. Bachmatiuk, M. H. Rümmeli
Electron Beam Emergent Additive Manufacturing (EBEAM Centre)
Institute of Environmental Technology (IET)
Centre for Energy and Environmental Technologies (CEET)
VSB—Technical University of Ostrava
17 Listopadu 15, 708 33 Ostrava, Czech
E-mail: mhr1@suda.edu.cn

M. H. Rümmeli
Jiangsu Key Laboratory of Advanced Negative Carbon Technologies
Soochow University
Suzhou, Jiangsu 215123, P. R. China

M. H. Rümmeli
Key Laboratory of Core Technology of High Specific Energy Battery and
Key Materials for Petroleum and Chemical Industry
Soochow University
Suzhou 215006, China

 Supporting information for this article is available on the WWW under <https://doi.org/10.1002/batt.202500185>

 © 2025 The Author(s). *Batteries & Supercaps* published by Wiley-VCH GmbH. This is an open access article under the terms of the Creative Commons Attribution License, which permits use, distribution and reproduction in any medium, provided the original work is properly cited.

additives to mitigate mechanical strain in electrode design has rarely been explored, despite being a crucial and essential part of electrode design. Recently, this field has gained significant attention, and an increasing number of researchers have investigated stress control strategies. Zhang et al.^[12] prepared microsized Si-rich particles as an anode by electric arc furnace melting and high-energy ball milling and realized a stress-relieving mechanism to stabilize anode performance. Shi presented novel hollow graphitic carbon (HGC) with customized dual dimensions as a functional conductive additive to regulate strain during lithiation in μ Si anodes.^[11e] With the introduction of elastic hollow graphite carbon shells for stress regulation, the μ Si anode exhibited stable electron and ion transport and enhanced lithium storage. However, the complexity of the preparation process of HGC hindered its commercialization.^[13]

Biomass materials have garnered significant interest for the development of LIBs owing to their sustainability, environmental benefits, and unique physicochemical properties.^[14] In this study, biomass-derived carbon microtubes (CMTs) were introduced into μ Si electrodes as elasticity mediators to alleviate the stress generated during cycling. The inherent tubular structure of kapok fibers offers a natural possibility for mitigating the volume expansion of the μ Si anode. Through the carbonization of kapok fibers at a moderate temperature, CMTs were formed, offering an innovative, bioinspired solution to further stabilize the μ Si anode. The organic components in the kapok fiber wall impart exceptional elasticity and resilience, enabling the CMTs to retain a resilient structure that can withstand the stress induced during lithiation, thus preventing severe electrode deformation. With only 2 wt% CMTs added, the electrode exhibited significantly improved lithium storage capabilities, achieving a remarkable capacity of

1047 mAh g⁻¹ after 200 cycles at a high current density of 2 A g⁻¹, which is significantly better than that of the pure μ Si electrode without the addition of CMTs.

2. Results and Discussion

2.1. Materials Characterization

Hollow-structured CMTs were prepared via a facile carbonization process, as illustrated in Scheme S1, Supporting Information.

Figure 1 shows the scanning electron microscopy (SEM) images and diameter distribution of the raw kapok and the CMTs annealed at 370 °C and 1000 °C. The raw kapok fibers have a large inner diameter of 16–18 μ m (Figure 1a,d,g). Figure 1b,e confirms that the size of the CMTs annealed at 370 °C is similar to that of raw kapok. Natural kapok fibers consist of 64% cellulose, 13% lignin,^[15] and so on. At significantly low carbonization temperature and duration, the fiber structure is not completely decomposed.^[16] As a result, the samples carbonized at 370 °C (denoted as Re-CMTs, resilient CMTs) with a kapok-like morphology maintain a certain mechanical resilience. The product carbonized at 1000 °C (denoted as Br-CMTs, brittle CMTs) experiences a greater loss of fibrous tissue, resulting in a reduced internal diameter (12–15 μ m, Figure 1c,f,h). Some become even more brittle, resulting in wall collapse and cracks at the open end (Figure S1, Supporting Information).

The X-ray diffraction (XRD) spectra of the Re-CMTs and Br-CMTs are shown in **Figure 2a** and that of kapok are shown in Figure S2, Supporting Information. The diffraction peaks located at \approx 21.7° correspond to the (0 0 2) plane of graphitic carbon.^[17]

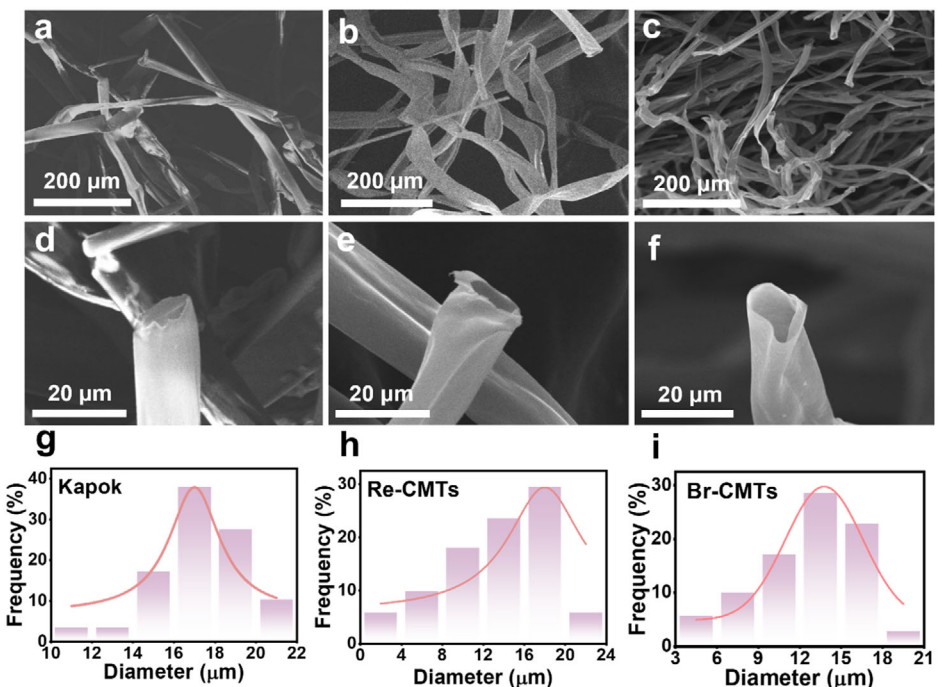


Figure 1. a,d) SEM images of kapok. b,e) SEM images of the Re-CMTs. c,f) SEM images of the Br-CMTs. Diameter distributions of g) kapok, h) Re-CMTs, and i) Br-CMTs.

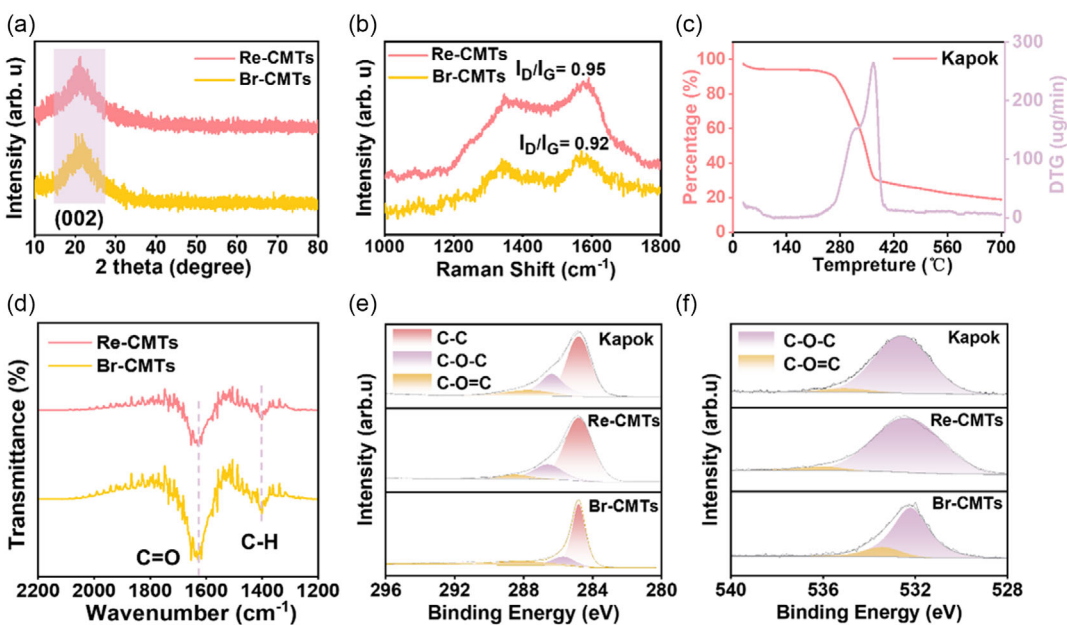


Figure 2. a) XRD patterns. b) Raman spectra. c) TGA measurements. d) FTIR spectra. XPS spectra of kapok and its carbonized samples, e) C 1s, and f) O 1s.

As the annealing temperature increases from 370 °C to 1000 °C, the strength increases slightly, indicating that a higher temperature leads to a higher degree of graphitization. Raman spectra further confirmed the graphitic structure of the carbonized samples (Figure 2b). Two peaks centered at 1346 cm⁻¹ and 1579 cm⁻¹ are attributed to the *D* (defect feature) and *G* (graphitic feature) bands, respectively.^[18] The *D/G* intensity ratios of the Re-CMTs (0.95) and Br-CMTs (0.92) suggest that the Re-CMTs had more disordered areas than the Br-CMTs, which could facilitate electrolyte infiltration and enhance lithium-ion transportation inside the electrode.

The onset decomposition temperature of kapok was measured to be ≈260 °C by thermogravimetric analysis (TGA). When the kapok is annealed to 370 °C in a nitrogen atmosphere to form Re-CMTs, 30% of the original components remain, which contributes to the elasticity of the tube wall (Figure 2c). In the fourier transform infrared spectroscopy (FTIR) spectrum (Figure 2d), the absorption peaks at 1600 cm⁻¹ and 1400 cm⁻¹ correspond to the C=O and C—H bending vibrations, respectively,^[14b] with Re-CMTs exhibiting significantly lower transmittance at 1600 cm⁻¹, indicating a higher C=O content in Re-CMTs. This increased C=O content can enhance molecular interactions, thereby contributing to the improved flexibility and elasticity of Re-CMTs.^[19]

The chemical compositions and surface concentrations of C, N, and O in the CMTs were investigated using X-ray photoelectron spectroscopy (XPS), and the results are shown in Figure 2e,f. Figure S3, Supporting Information, shows the XPS survey spectra of the CMTs. All the binding energies (E_b) were calibrated to the C 1s peak at 284.80 eV. The C 1s spectra (Figure 2e) exhibit three distinct peaks, corresponding to C—C (284.8 eV), C—O—C (286.24 eV), and C=O—C (288.4 eV). Additionally, the high-resolution O 1s XPS spectra showed consistent peaks corresponding to the C—O—C and C=O—C bonding. The relative content of the oxygen functionalities of the Br-CMTs decreased compared to

that of the Re-CMTs, indicating that the elasticity of the Re-CMTs may be associated with a higher organic content. The N1s spectra are shown in Figure S4, Supporting Information. To evaluate the elasticity and resilience of the Re-CMTs and their potential effects on stress regulation in the electrodes, the Young's modulus and mechanical behavior of the electrodes containing Re-CMTs were measured using atomic force microscopy (AFM). The as-prepared electrodes are denoted as Si/Re-CMTs and Si/Br-CMTs, and a pure Si electrode without CMTs was fabricated as a control sample. The AFM images and distribution of the Young's modulus for Si/Re-CMT (a, d), Si/Br-CMT (b, e), and pure Si electrodes (c, f) in the fresh state are shown in Figure 3. The Si/Re-CMTs electrode exhibited the lowest elastic modulus (8–12 GPa), which can be attributed to the notable elasticity and resilience of Re-CMTs. From this result, we can assume that Re-CMTs can effectively absorb internal stress and reduce the overall stiffness of the electrode. In contrast, the elastic modulus of the Si/Br-CMTs was moderate, ranging from 10 to 14 GPa. Consequently, Br-CMTs exhibited increased brittleness and retained only a limited degree of flexibility. The pure Si electrode, with the highest elastic modulus (20–36 GPa), is more rigid, which may lead to increased local stress accumulation, cracks, and structural damage during charge and discharge cycles, adversely affecting cycle stability. The addition of CMTs endowed the electrodes with elasticity and compressive resistance, which were further evaluated using an electrode resistance meter. As shown in Figure 3g, the percentage changes in the thicknesses of the three electrodes at various pressures are depicted. Starting at 5 MPa, the pressure was gradually increased by 3 MPa every 15 s, reaching 60 MPa, and then decreased to 5 MPa. During the pressurization process, the overall thickness of the electrodes progressively shrank (Figure S5, Supporting Information). Si/Re-CMTs had the largest reversible variable among them, at 3.49% (Figure 3h). This is attributable to the introduction of the Re-CMTs, which

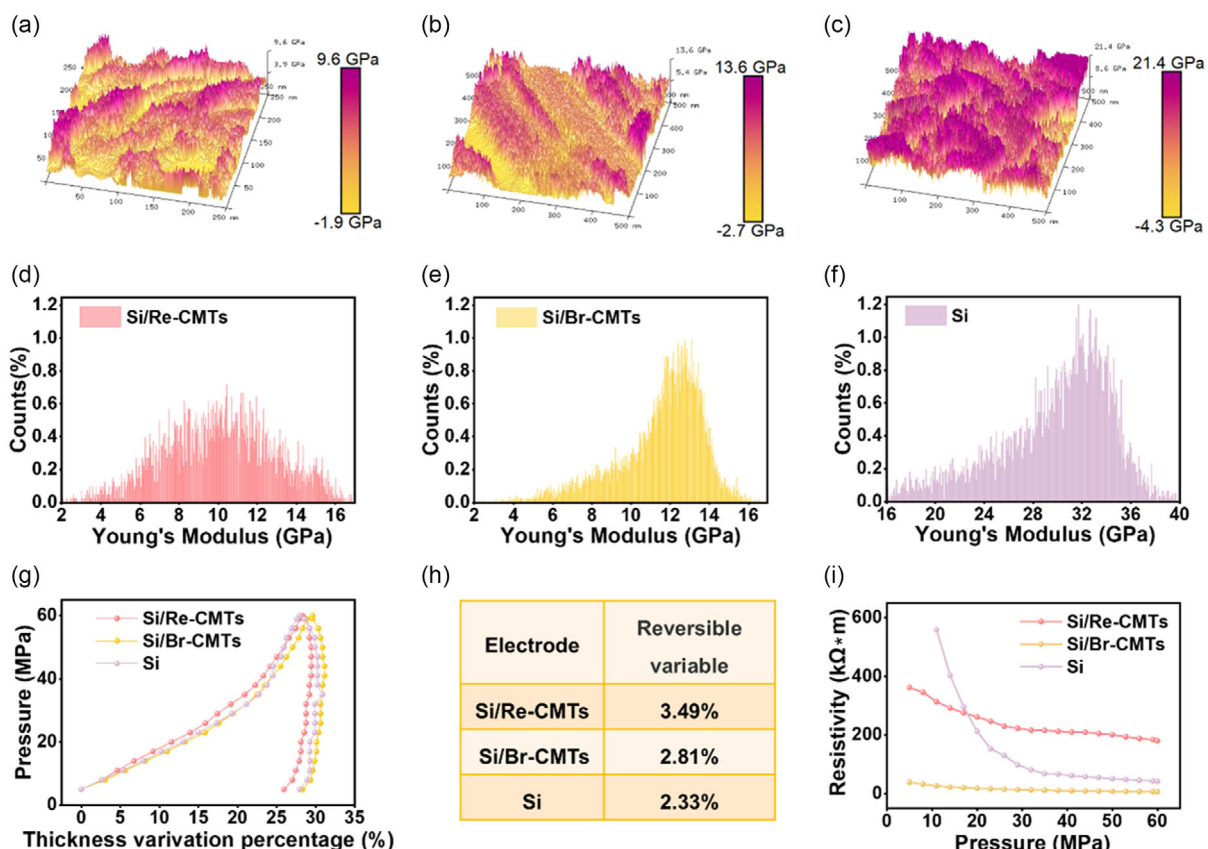


Figure 3. a,d) The AFM 3D images and Young's modulus distribution of the Si/Re-CMTs, b,e) Si/Br-CMTs, and c,f) Si electrodes at the fresh stage. g) Pressure versus thickness variation percentage for Si/Re-CMTs, Si/Br-CMTs, and Si. h) Reversible variation for Si/Re-CMTs, Si/Br-CMTs, and Si. i) Resistivity versus pressure for Si/Re-CMTs, Si/Br-CMTs, and Si.

facilitated the elastic recovery of the entire electrode, thereby showcasing their substantial potential for mitigating stress. The reversible deformation of Si/Br-CMTs was 2.81%, better than that of pure silicon without an elastic medium, which is 2.33%. Throughout the pressurization process, the resistivities of the three electrodes exhibited a declining trend (Figure 3i). As it is outside this range, the resistivity data for the pure Si electrode at 5 MPa and 8 MPa are absent. Br-CMTs exhibit higher conductivity than Re-CMTs carbonized at 370 °C due to a more extensive carbonization degree. The resistivity of the Si electrode decreased progressively as the pressure increased to 20 MPa. This is because the increasing pressure gradually compressed the pores inside the Si electrode, thus improving the electrical connection. Re-CMTs can bear gradually increasing pressures, avoiding further compression of the electrode porosity. Consequently, the resistivity of the Si/Re-CMTs was stable at a constant value above 20 MPa.

2.2. Electrochemical Performance

Electrochemical performance tests were conducted to verify the strain regulation effect of the CMTs on μ Si anodes. The three electrodes were assembled into half cells and tested under the same conditions. Cyclic voltammetry (CV) was conducted to examine the electrochemical response of the three electrodes within the voltage window of 0.01–2.0 V at a scan rate of 0.2 mV s⁻¹. As shown in

the CV curves of the Si/Re-CMTs and Si/Br-CMTs electrodes (Figure 4a,b), a broad cathodic peak near 1.7 V indicates the formation of SEI due to electrolyte decomposition. This peak disappeared in subsequent cycles, suggesting the formation of a stable SEI after the first cycle. The Si/Re-CMTs and Si/Br-CMTs display a higher intensity of the SEI-related peak than the Si electrode, which is attributed to the large surface area of the CMTs, enabling greater infiltration of the electrolyte. Additionally, the transition of crystalline silicon to amorphous lithium silicide (Li_xSi) upon lithium intercalation is indicated by the peak observed at 0.1 V in the first cathodic scan.^[20] The anodic sweeps show two faint peaks at 0.3 V and 0.60 V, which are attributable to Li_xSi de-lithiation to amorphous Si at the electrode. The current response was enhanced in the subsequent cycles, which may be attributed to electrolyte infiltration and full activation of the electrode. The CV curves of the Si/Re-CMTs electrode almost overlapped during the second and third cycles, indicating that the electrochemical reaction on the electrode surface had stabilized. This behavior indicates that CMTs facilitate in mitigating the stress incurred during the lithiation of μ Si, reducing the volume expansion of Si and enhancing the reversibility and cycle stability. In contrast, the samples without CMTs exhibit poor reversibility, likely due to the expansion of Si and the absence of a robust conductive network (Figure 4c).

Figure 4d shows the galvanostatic charge–discharge curves of the three electrodes during the 1st cycle. The voltage platforms during charge/discharge were consistent with the observed CV

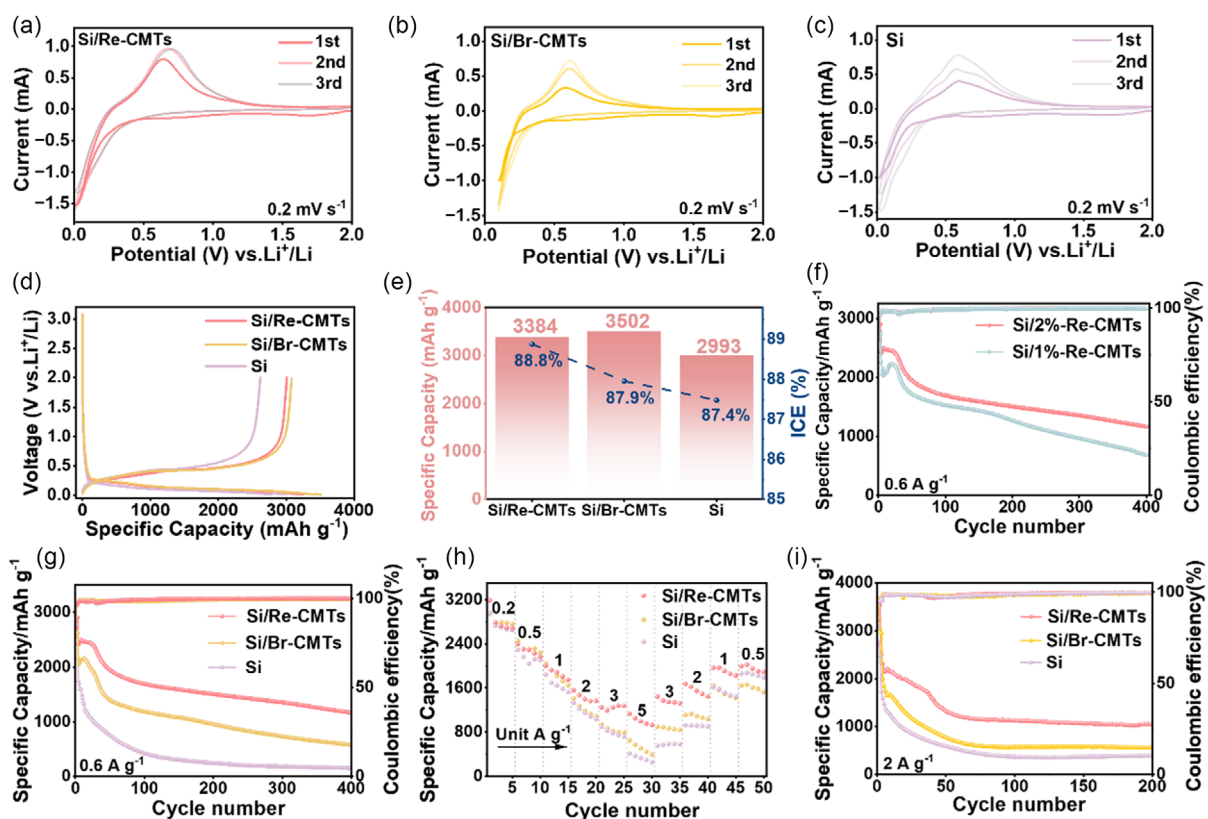


Figure 4. CV curves of a) Si/Re-CMTs, b) Si/Br-CMTs, and c) Si electrodes for the first three cycles performed at a scan rate of 0.2 mV s^{-1} d) Voltage profiles at the first cycle; e) ICE and first discharge capacity. f) Long-term cycling performance of Si/Re-CMTs with various Re-CMTs ratios at a current density of 0.6 A g^{-1} , g) long-term cycling performance at a current density of 0.6 A g^{-1} , h) rate capability, and i) long-term cycling performance at a high current density of 2 A g^{-1} .

curves. As shown in Figure 4e, the Si electrode exhibits a relatively low initial discharge capacity (2993 mAh g^{-1}). In contrast, the initial discharge capacities of the Si/Re-CMTs and Si/Br-CMTs electrodes are 3384 mAh g^{-1} and 3502 mAh g^{-1} respectively. This significant increase in the reversible capacity demonstrates the effectiveness of incorporating CMTs into the electrode. In addition, the Si/Br-CMTs electrode had the highest initial coulombic efficiency (ICE) (88.8%), exceeding 87.9% for the Si/Re-CMTs electrode and 87.5% for the Si electrode. After proving the effectiveness of the CMTs, their rational proportions were further examined. The addition of 2% CMTs to the slurry resulted in higher electrochemical performance than that of 1% CMTs (Figure 4f), prompting the decision to adopt a 2% CMT ratio as the working electrode in the following characterizations. In the long-term cycling test at a current density of 0.6 A g^{-1} , Si/Re-CMTs exhibit significantly better stability compared to Si/Br-CMTs and Si electrode. After 400 cycles, Si/Re-CMTs and Si/Br-CMTs deliver a discharge capacity of $1164.0 \text{ mAh g}^{-1}$ and 574.8 mAh g^{-1} respectively (Figure 4g). The excellent performance of the Si/Re-CMTs electrode demonstrates the greater effectiveness of Re-CMTs in mitigating volume expansion than Br-CMTs. For comparison, the Si anode undergoes rapid capacity decay and retains a capacity of 156 mAh g^{-1} after 400 cycles. Upon increasing the current density from 0.5 to 5 A g^{-1} the Si/Re-CMTs and Si/Br-CMTs electrodes consistently demonstrate a higher lithium storage capacity at each current density (Figure 4h). When the current density decreased

back to 0.5 A g^{-1} , the specific capacity of the Si/Re-CMTs recovered to $1852.6 \text{ mAh g}^{-1}$, demonstrating the superior rate performance of the electrodes and the stress-relief capability of the CMTs. In contrast, Si electrodes exhibit poor cycle stability and rate capability. Without CMTs to alleviate the stress, the electrode failed to buffer the volume changes in Si, leading to rapid electrode degradation. When tested at a high current density of 2 A g^{-1} (Figure 4i), the Si/Re-CMTs and Si/Br-CMTs electrodes achieve relatively higher capacities of 1047 mAh g^{-1} and 564 mAh g^{-1} respectively, while the Si electrode retains only a negligibly low capacity. The electrochemical performance at a higher current density of 3 A g^{-1} is shown in Figure S6, Supporting Information.

2.3. Structure and Kinetics Evolution

To investigate the kinetic evolutions of the three distinct electrodes, the electrochemical impedance spectra (EIS) of the electrodes (Figure 5a–c) were obtained in the initial state and after 10, 20, 50, and 100 cycles. An equivalent circuit model (Figure S7, Supporting Information) was used to fit the recorded EIS spectra. This model includes several key components: R_s represents the ionic resistance of the electrolyte in the high-frequency region, R_{SEI} is associated with the resistance of Li^+ migration through the SEI in the high-frequency region, R_{CT} points to the resistance of charge transfer in the mid-frequency region, and Z_w

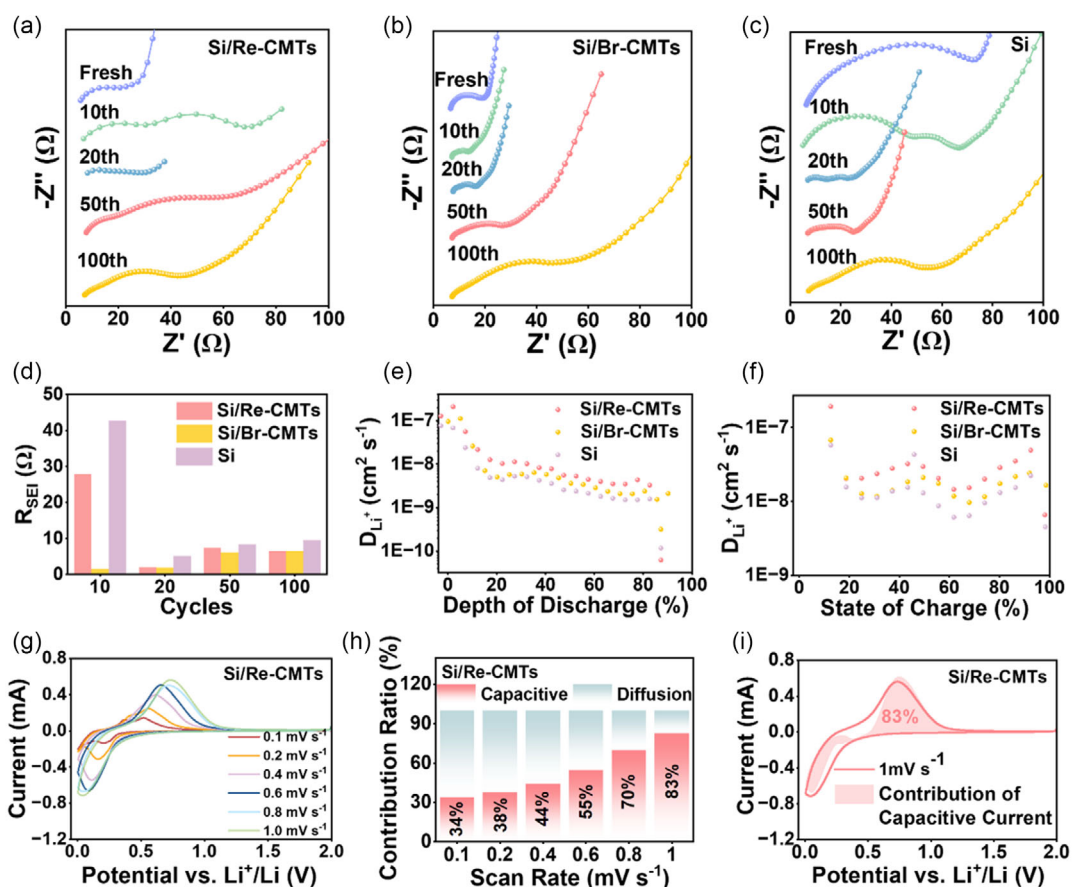


Figure 5. Ex situ EIS measurements of a) Si/Re-CMTs, b) Si/Br-CMTs, and c) Si electrodes in the fresh state after 10, 20, and 50 cycles and after 100 cycles. d) R_{SEI} statistics for Si/Re-CMTs, Si/Br-CMTs, and Si electrodes under different cycling conditions. Calculated Li-ion diffusion coefficients during e) the discharge and f) charge processes. g) CV curves of Si/Re-CMTs anode at different scan rates. h) Contribution ratios of capacitance and diffusion processes to capacity at different scanning rates. i) CV curve and capacitive current contribution at 1 mV s⁻¹.

(the Warburg impedance, associated with the Li^+ diffusion coefficient) in the low-frequency region.

As shown in Figure 5d, the R_{SEI} of the Si/Re-CMTs electrode initially peaked at the 10th cycle, decreased, and gradually stabilized with further cycling. This trend can be explained by the fact that the introduction of Re-CMTs reduces the volume expansion rate; thus, the SEI gradually stabilizes, and the side reactions are suppressed. Additionally, the superior conductivity of Br-CMTs resulted in a relatively lower R_{SEI} (Figure 5d). In contrast, after 100 cycles, the R_{SEI} of the Si electrodes without CMTs rises to 200 Ω . The primary reason for this is the severe volume expansion of Si during cycling, which fractures the Si and exposes new surfaces. This exposure leads to excessive electrolyte decomposition, resulting in an unstable thick SEI. Additionally, the detachment of Si particles results in the loss of electrical contact with the conductive matrix, which significantly impedes electron transfer. This disconnection increases the overall electron transfer resistance of the electrode, which exacerbates its cycle stability and causes a serious R_{SEI} rise. The specific values of R_{ct} and R_e are presented in Figure S8, Supporting Information.

To analyze the dynamic behavior of the three electrodes and further explore their kinetics, the galvanostatic intermittent titration technique was conducted with a pulse current of 400 mA g⁻¹ for 30 min with a 3 h rest (Figure S9, Supporting Information).

As shown in Figure 5e,f, the calculated D_{Li^+} results indicate that the Si/Re-CMTs and Si/Br-CMTs electrodes exhibited higher D_{Li^+} values than those of the Si electrode during both the charging and discharging processes. This improvement can be attributed to the larger transport channels provided by the CMTs, which likely enhanced the rate of Li^+ diffusion in the Si/Re-CMTs and Si/Br-CMTs.

The pseudocapacitive contributions of the three electrodes were calculated using the CV curves at scan rates of 0.1, 0.2, 0.4, 0.6, 0.8, and 1.0 mV s⁻¹ (Figure 5g). As the scan rate increases, the anodic and cathodic peaks shift to higher and lower potentials, respectively. The peak current (i) varied with the scan rate (v), as described by the power-law equation: $\log(i) = \log(a) + b \log(v)$.^[21] The b value was used to assess the diffusion-controlled and capacitive contributions to the electrochemical behavior. A b value close to 1 indicates a process dominated by capacitive behavior and rapid kinetics. The fitted b values for peaks O and R, based on the relationship between i and v , are calculated to be 0.57 and 0.6, respectively (Figure S10, Supporting Information). These relatively high b values suggest that the lithium storage capacity of the Si/Re-CMTs was primarily due to capacitive processes with fast kinetics. The current (i) at a fixed potential (V) can be expressed as the sum of a capacitive-controlled process ($k_1 v$) and a diffusion-controlled process ($k_2 V^{1/2}$) using the equation: $i = k_1 v + k_2 V^{1/2}$.^[22]

By determining k_1 and k_2 , the contribution of each process at specific scan rates was quantified (Figure 5h). At 0.1 mV s^{-1} , the capacitive-controlled process contributes 34% of the total capacity. As the scan rate increases, the capacitive contribution gradually dominates, reaching 83% at 1.0 mV s^{-1} (Figure 5i). For comparison, the pseudocapacitive data of the Si/Br-CMTs and Si electrodes are shown in Figure S11 and S12, Supporting information.

The XPS of the three electrodes after 500 cycles are presented in Figure 6. In Figure 6a, the C 1s spectrum of Si electrode reveals an increase in organic components containing C—C, C—O, and C=O bonds at 284.8, 286, and 289.1 eV, as well as 531 eV of C=O and 532.9 eV of C—O in the O 1s spectra, consisting of lithium alkyl carbonates such as lithium ethylene decarbonate (LEDC), lithium methyl carbonate (LMC), lithium ethyl carbonate (LEC), and their oligomers.^[23] These organic components usually have low ionic conductivities, which negatively affect the electrochemical stability of pure Si electrodes. A stronger lithium carbonate (Li_2CO_3) signal in the C 1s spectra (290.2 eV, Figure 6a) and stronger lithium oxide (Li_2O) in the O 1s spectra (529.8 eV, Figure 6b) in the Si/Re-CMTs electrode indicate that Re-CMTs promote homogenous Li^+ flux and facilitate ion transport through the electrode-electrolyte interface. Furthermore, the increased intensity of the lithium fluoride (LiF) peak in the Si/Re-CMTs electrode compared

to that of the pure Si electrode (Figure 6c) suggests that Re-CMTs facilitate the formation of a LiF-rich SEI (Figure 6d), thus restraining unfavorable interfacial side reactions.^[24]

To confirm capacity of the CMTs to reduce the volume expansion during lithiation, the thickness variations of the electrodes extracted from the cycled batteries at different discharge depths were evaluated using cross-sectional imaging with SEM. The cycled batteries were disassembled in an Ar-filled glove box. The aged electrodes were rinsed three times with dimethyl carbonate (DMC), dried overnight at 80°C under vacuum, and then swiftly transferred to the SEM to avoid contamination by air or moisture. Figure S13, Supporting Information, shows the cross-sectional morphologies of the Si/Re-CMTs (Figure S13a–f, Supporting Information), Si/Br-CMTs (Figure S13g–l, Supporting Information), and Si electrode (Figure S13m–r, Supporting Information) in the fresh state and after 20%, 40%, 60%, 80%, and complete lithiation, respectively. Figure 6e shows the rate of change in the thickness of the three electrodes at different discharge depths. It can be observed that Si/Re-CMTs experienced the smallest change in the thickness, and Br-CMTs were less resistant to stress due to the more brittle tube wall, indicating that Re-CMTs play a significant role in strain management. The surface morphologies in the fresh state and after different discharge depths for the three

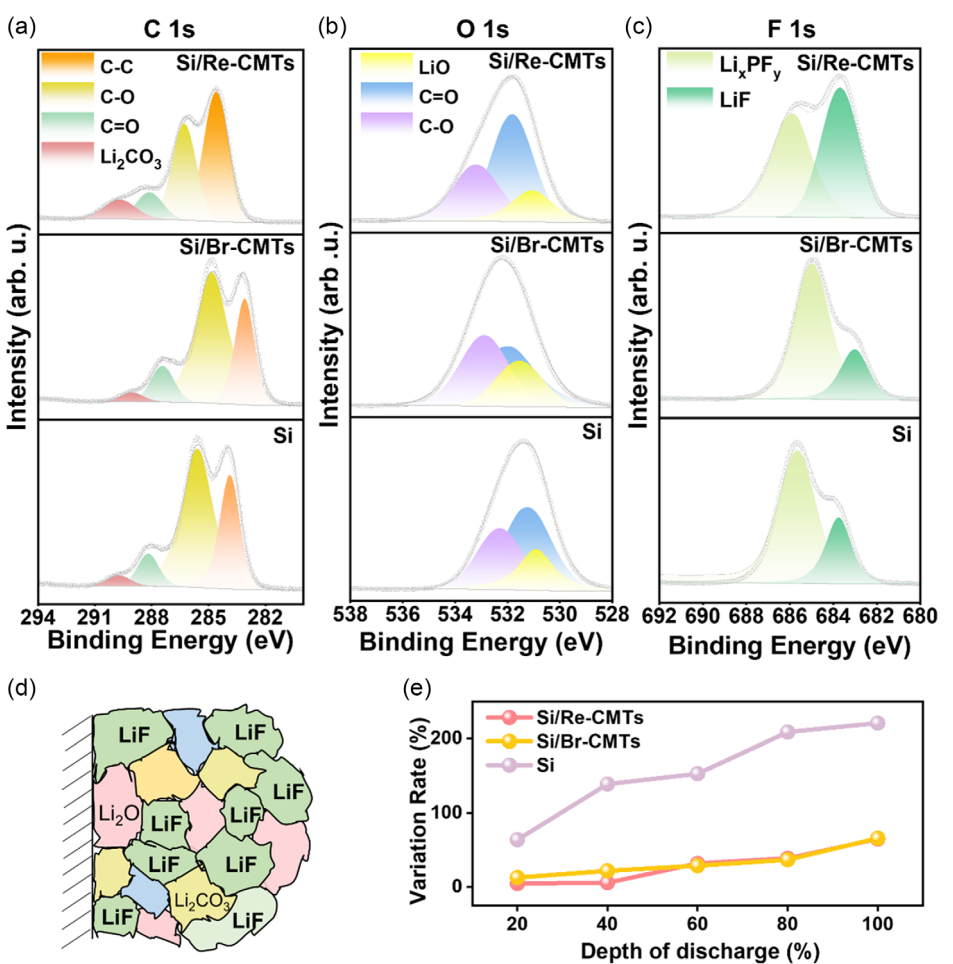


Figure 6. XPS characterization of a) Si/Re-CMTs, b) Si/Br-CMTs, and c) Si electrodes after 500 cycles. d) The formation of LiF-rich SEI. e) Thickness variation rate of the three electrodes at different discharge depths.

electrodes are shown in Figure S14, Supporting Information. The Si/Re-CMTs (Figure S14a–d, Supporting Information) and Si/Br-CMTs electrodes (Figure S14, e–h, Supporting Information) maintained their surface integrity at different discharge depths. However, in the aged electrode of pure Si, large cracks were observed at 80% and 100% discharge depths (Figure S14k,l, Supporting Information), which inevitably led to a large area of active material falling off from the current collector and loss of electrical connection during cycling, resulting in poor electrochemical performance.

Modulus analyses of the three electrodes after 500 cycles were conducted using AFM. According to the results, after 500 cycles, the modulus of the Si/Re-CMTs remained the smallest (150–250 MPa) (Figure S15b,c, Supporting Information), which was smaller than Si/Br-CMTs (300–400 MPa) (Figure S15e,f, Supporting Information) and the Si electrode (350–500 MPa) (Figure S15h,i, Supporting Information). The low modulus of the Si/Re-CMTs electrode indicated that the Re-CMTs absorbed the mechanical stress generated by the volume expansion. SEM images of Si/Re-CMTs and Si/Br-CMTs electrodes after 500 cycles are shown in Figure S15, Supporting Information and, d, where no significant cracking was observed on the electrode surface. However, as shown in Figure S15g, Supporting Information, a large crack was generated on the Si electrode after 500 cycles, which may have resulted in poor cycle stability.

3. Conclusion

In this study, biomass-derived stress-regulating additives, namely partially carbonized microtubes (Re-CMTs), were elaborately designed and successfully applied to regulate the stress in μ Si anodes, effectively alleviating volume expansion, offering a more environmentally friendly approach to enhancing battery performance. The reserved organic compositions in the CMTs architecture endow them with enhanced elasticity, and their inner voids alleviate local stress accumulation. Consequently, the Si/Re-CMTs anode exhibited a reversible specific capacity of 1047 mAh g⁻¹ at a high current density of 2 A g⁻¹. Various postanalysis results showed that the addition of Re-CMTs played a key role in regulating strain evolution and accelerating electrochemical reaction kinetics. In addition, the preparation of stress-regulating additives is simple, effective, and environmentally friendly and requires no additional modification, making biomass-derived Re-CMTs promising candidates for accelerating the commercial application of microsized silicon-based anodes.

4. Experimental Section

Synthesis of CMTs

5 g kapok powders were washed several times with ethanol and deionized water to remove surface dust and dried at 80 °C overnight in a vacuum oven. Then, 5 g of dried kapok powders were heated to 370 °C and 1000 °C, respectively, for 30 min at a rate of 20 °C min⁻¹ under an Ar atmosphere. After carbonization, black products (\approx 0.5 g) were collected.

Electrode Preparation

The working electrode (Si/Re-CMTs and Si/Br-CMTs) consisted of 70 wt% μ Si, 15 wt% lithium polyacrylate (PAALi, 4 wt%, Guangdong, Canrd New Energy Technology Co., Ltd.) binder, 2 wt% Re-CMTs/Br-CMTs, and 13 wt% super P. The control sample (Si) consisted of 70 wt% μ Si, 15 wt% PAALi, and 15 wt% Super P. The μ Si and conductive additive powders were first mixed by hand milling in mortar. The slurry was prepared by mixing the obtained powders with PAALi binder in a vial by magnetic stirring for 5 h and was further coated on the Cu foil by a doctor blade and dried at 60 °C to remove the moisture. The as-prepared electrode was cut into 14 mm discs followed by vacuum drying at 80 °C overnight.

Supporting Information

Supporting Information is available from the Wiley Online Library or the author.

Acknowledgements

M.H.R. thanks the National Natural Science Foundation of China (grant no. 52071225) and the European Union's Horizon Europe Research and Innovation Program under grant agreement no. 101087143 (Electron Beam Emergent Additive Manufacturing (EBEAM)) under the RE-FRESH, Research Excellence For Region Sustainability and High-tech Industries (project no. CZ.10.03.01/00/22_003/0000048) through an operational program transition. Y.S. thanks the National Key R&D Program of China (2021YFB3800300) and the National Natural Science Foundation of China (grant nos. 22179143 and 22002176). Q.S. thanks the Jiangsu Funding Program for Excellent Postdoctoral Talent. A.B. thanks the Norway grant project no. 2019/34/H/ST8/00547 through the National Science Centre.

Open access publishing facilitated by Vysoka skola banska-Technicka univerzita Ostrava, as part of the Wiley - CzechELib agreement.

Conflict of Interest

The authors declare no conflict of interest.

Author Contributions

Luwen Li: conceptualization (equal); data curation (lead); formal analysis (equal); investigation (Lead); methodology (equal); project administration (equal); writing—original draft (equal). **Qitao Shi:** conceptualization (equal); data curation (equal); formal analysis (equal); supervision (equal); writing—original draft (equal); writing—review and editing (supporting). **Zhipeng Wang:** data curation (supporting); formal analysis (supporting); investigation (supporting); methodology (supporting); writing—original draft (supporting). **Cheng Zhang:** data curation (supporting); formal analysis (supporting); investigation (supporting); methodology (supporting). **Jiaqi Wang:** data curation (supporting); formal analysis (supporting); investigation (supporting); methodology

(supporting); writing—original draft (supporting). **Junjin Zhang:** data curation (supporting); formal analysis (supporting); investigation (supporting); methodology (supporting). **Xiangqi Liu:** data curation (supporting); formal analysis (supporting); methodology (supporting); project administration (supporting). **Alicja Bachmatiuk:** data curation (supporting); methodology (supporting); resources (supporting); supervision (supporting); writing—review and editing (supporting). **Ruiwei Yang:** formal analysis (supporting); investigation (supporting); supervision (supporting); writing—original draft (supporting). **Yanbin Shen:** conceptualization (supporting); data curation (supporting); resources (supporting); writing—original draft (supporting). **Mark H. Rümmeli:** conceptualization (equal); data curation (equal); formal analysis (equal); funding acquisition (lead); resources (equal); supervision (equal); writing—original draft (lead); writing—review and editing (lead). **Luwen Li** and **Qitao Shi** contributed equally to this work.

Data Availability Statement

The data that support the findings of this study are available from the corresponding author upon reasonable request.

Keywords: resilient carbon microtubes • Si anodes • stress-regulating additives

- [1] a) L. Sun, Y. Liu, L. Wang, Z. Jin, *Adv. Funct. Mater.* **2024**, *34*, 2403032; b) J. M. Tarascon, M. Armand, *Nature* **2001**, *414*, 359.
- [2] a) Z. Zhao, F. Chen, J. Han, D. Kong, S. Pan, J. Xiao, S. Wu, Q. H. Yang, *Adv. Energy Mater.* **2023**, *13*, 2300367; b) Q. Shi, J. Zhou, S. Ullah, X. Yang, K. Tokarska, B. Trzebicka, H. Q. Ta, M. H. Rümmeli, *Energy Storage Mater.* **2021**, *34*, 735.
- [3] a) W. Wang, F. Xiong, S. Zhu, J. Chen, J. Xie, Q. An, *eScience* **2022**, *2*, 278; b) Y. Yang, Z. Yang, Z. Li, J. Wang, X. He, H. Zhao, *Adv. Energy Mater.* **2023**, *13*, 2302068.
- [4] a) L. Ye, Y. Lu, Y. Wang, J. Li, X. Li, *Nat. Mater.* **2024**, *23*, 244; b) J. W. Choi, D. Aurbach, *Nat. Rev. Mater.* **2016**, *1*, 16013; c) L. Sun, Y. Liu, L. Wang, Z. Jin, *Adv. Funct. Mater.* **2024**, *34*, 2403032.
- [5] a) X. Su, Q. Wu, J. Li, X. Xiao, A. Lott, W. Lu, B. W. Sheldon, J. Wu, *Adv. Energy Mater.* **2014**, *4*, 1300882; b) H. Kim, M. Seo, M.-H. Park, J. Cho, *Angew. Chem. Int. Ed.* **2010**, *49*, 2146; c) X. H. Liu, H. Zheng, L. Zhong, S. Huang, K. Karki, L. Q. Zhang, Y. Liu, A. Kushima, W. T. Liang, J. W. Wang, J.-H. Cho, E. Epstein, S. A. Dayeh, S. T. Picraux, T. Zhu, J. Li, J. P. Sullivan, J. Cumings, C. Wang, S. X. Mao, Z. Z. Ye, S. Zhang, J. Y. Huang, *Nano Lett.* **2011**, *11*, 3312; d) Y. Wei, T. Wang, J. Wang, S. Wang, D. Zhang, Y. Ma, Y. Gao, L. Duan, D. Yang, W. Zhang, *Small Methods* **2024**, *8*, 2400069.
- [6] a) N. Liu, H. Wu, M. T. McDowell, Y. Yao, C. Wang, Y. Cui, *Nano Lett.* **2012**, *12*, 3315; b) N. Liu, Z. Lu, J. Zhao, M. T. McDowell, H.-W. Lee, W. Zhao, Y. Cui, *Nat. Nanotechnol.* **2014**, *9*, 187; c) Q. Xu, J. Y. Li, J. K. Sun, Y. X. Yin, L. J. Wan, Y. G. Guo, *Adv. Energy Mater.* **2017**, *7*, 1601481.
- [7] a) J. H. Ryu, J. Kim, Y.-E. Sung, S. Oh, *Electrochim. Solid State Lett.* **2004**, *7*, A306; b) D. H. S. Tan, Y.-T. Chen, H. Yang, W. Bao, B. Sreenarayanan, J.-M. Doux, W. Li, B. Lu, S.-Y. Ham, B. Sayahpour, J. Scharf, E. A. Wu, G. Deysher, H. E. Han, H. J. Hahn, H. Jeong, J. B. Lee, Z. Chen, Y. S. Meng, *Science* **2021**, *373*, 1494; c) L. Gu, J. Han, M. Chen, W. Zhou, X. Wang, M. Xu, H. Lin, H. Liu, H. Chen, J. Chen, Q. Zhang, X. Han, *Energy Storage Mater.* **2022**, *52*, 547.
- [8] a) X. Peng, B. Liu, J. Chen, Q. Jian, Y. Li, T. Zhao, *ACS Energy Lett.* **2023**, *8*, 3586; b) A.-M. Li, Z. Wang, T. Lee, N. Zhang, T. Li, W. Zhang, C. Jayawardhana, M. Yeddala, B. L. Lucht, C. Wang, *Nat. Energy* **2024**, *9*, 1551; c) Q. Li, J. Ruan, S. Weng, X. Zhang, J. Hu, H. Li, D. Sun, X. Wang, F. Fang, F. Wang, *Angew. Chem. Int. Ed.* **2023**, *62*, e202310297; d) Y. Wang, T. Li, X. Yang, Q. Yin, S. Wang, H. Zhang, X. Li, *Adv. Energy Mater.* **2024**, *14*, 2303189.
- [9] a) S. Choi, T.-W. Kwon, A. Coskun, J. W. Choi, *Science* **2017**, *357*, 279; b) T. Munaoka, X. Yan, J. Lopez, J. W. F. To, J. Park, J. B. H. Tok, Y. Cui, Z. Bao, *Adv. Energy Mater.* **2018**, *8*, 1703138; c) D. Lusztig, S. Luski, N. Shpigel, N. Vangapally, D. Aurbach, *Batteries Supercaps* **2024**, *7*, e202400255.
- [10] a) H. Jia, X. Li, J. Song, X. Zhang, L. Luo, Y. He, B. Li, Y. Cai, S. Hu, X. Xiao, C. Wang, K. M. Rosso, R. Yi, R. Patel, J.-G. Zhang, *Nat. Commun.* **2020**, *11*, 1474; b) Y. Li, K. Yan, H.-W. Lee, Z. Lu, N. Liu, Y. Cui, *Nat. Energy* **2016**, *1*, 15029; c) D. Wang, Y. Ma, W. Xu, S. Zhang, B. Wang, L. Zhi, X. Li, *Adv. Mater.* **2023**, *35*, 2212157; d) W. Li, J.-H. Wang, Y. Li, H. Hsueh, X. Liu, Y. Zhao, S. Huang, X. Li, H.-M. Cheng, X. Duan, H. S. Park, *J. Am. Chem. Soc.* **2024**, *146*, 21320; e) Z. Zhao, J. Han, F. Chen, J. Xiao, Y. Zhao, Y. Zhang, D. Kong, Z. Weng, S. Wu, Q.-H. Yang, *Adv. Energy Mater.* **2022**, *12*, 2103565; f) Y. Zhang, W. Tang, H. Gao, M. Li, H. Wan, X. Kong, X. Liu, G. Chen, Z. Chen, *ACS Nano* **2024**, *18*, 15671; g) Z. Xiao, X. Lin, C. Zhang, J. Shen, R. Zhang, Z. He, Z. Lin, H. Jiang, F. Wei, *Small Methods* **2023**, *7*, 2201623; h) M. C. Schulze, K. Fink, J. Palmer, G. M. Carroll, N. S. Dutta, C. Zwiefel, C. Engtrakul, S.-D. Han, N. R. Neale, B. J. Tremolet de Villiers, *Batteries Supercaps* **2023**, *6*, e202300186; i) L. Sun, X. Jiang, Z. Jin, *Chem. Eng. J.* **2023**, *474*, 145960; j) X. Shi, X. Bi, T. Tang, J. Gu, Y. Lu, H. Jing, J. Xu, J. Yang, J. Wang, Z. Zhang, Y. Peng, *Batteries Supercaps* **2024**, *7*, e202400130; k) J. Xie, L. Sun, Y. Liu, X. Xi, R. Chen, Z. Jin, *Nano Res.* **2022**, *15*, 395; l) L. Sun, J. Xie, S. Huang, Y. Liu, L. Zhang, J. Wu, Z. Jin, *Sci. China Mater.* **2022**, *65*, 51.
- [11] a) B. Zhang, D. Liu, H. Xie, D. Wang, C. Hu, L. Dai, *J. Power Sources* **2022**, *539*, 231591; b) G. Lee, Y. Choi, H. Ji, J. Y. Kim, J. P. Kim, J. Kang, O. Kwon, D. W. Kim, J. H. Park, *Carbon* **2023**, *202*, 12; c) H. Zhang, S. Liu, X. Yu, S. Chen, *J. Alloys Compd.* **2020**, *822*, 153664; d) Q. Liu, W. Tang, C. Yang, W. Cai, F. Chen, Q. Fu, *Chem. Commun.* **2023**, *59*, 7435; e) Q. Shi, Y. Cheng, J. Wang, J. Zhou, H. Q. Ta, X. Lian, K. Kurtyka, B. Trzebicka, T. Gemming, M. H. Rümmeli, *Small* **2023**, *19*, 2205284; f) L. A. Dold, C. R. Bapat, H. Gentischer, N. Ortlieb, A. Fischer, K. P. Birke, D. Biro, *Batteries Supercaps* **2024**, *7*, e202400012.
- [12] Y. Gao, L. Fan, R. Zhou, X. Du, Z. Jiao, B. Zhang, *Nano-Micro Lett.* **2023**, *15*, 222.
- [13] X. Yu, J. Xiang, Q. Shi, L. Li, J. Wang, X. Liu, C. Zhang, Z. Wang, J. Zhang, H. Hu, A. Bachmatiuk, B. Trzebicka, J. Chen, T. Guo, Y. Shen, J. Choi, C. Huang, M. H. Rümmeli, *Small* **2024**, *20*, 2406309.
- [14] a) A. Kumar, T. Bhattacharya, S. M. Mozammil Hasnain, A. Kumar Nayak, M. S. Hasnain, *Mater. Sci. Energy Technol.* **2020**, *3*, 905; b) F. Li, J. Yang, J. Liao, S. Li, J. Liao, R. Prabhu, L. N. Williams, Y. Yang, J. Tang, N. Liu, *Chem. Eng. J.* **2015**, *276*, 322.
- [15] O. K. Sunmonu, D. Abdullahi, *J. Text. Inst.* **1992**, *83*, 273.
- [16] X.-Y. Zhang, C.-T. Duan, N. Zhao, H. Xiao, M.-W. Shi, X.-L. Zhang, J. Xu, *Chin. J. Polym. Sci.* **2010**, *28*, 841.
- [17] a) C. F. Holder, R. E. Schaak, *ACS Nano* **2019**, *13*, 7359; b) M. H. Rümmeli, C. Kramberger, A. Grüneis, P. Ayala, T. Gemming, B. Büchner, T. Pichler, *Chem. Mater.* **2007**, *19*, 4105.
- [18] M. H. Rümmeli, A. Bachmatiuk, A. Scott, F. Börrnert, J. H. Warner, V. Hoffman, J.-H. Lin, G. Cuniberti, B. Büchner, *ACS Nano* **2010**, *4*, 4206.
- [19] a) G. Xu, L. Jin, L. Ying, F. Wang, *J. Text. Inst.* **2011**, *102*, 120; b) O. K. Sunmonu, D. Abdullahi, *J. Text. Inst.* **1992**, *83*, 273.
- [20] a) Q. Shi, W. Ye, K. Kurtyka, H. Wang, X. Lian, H. Q. Ta, J. Zhou, X. Yang, L. Guo, B. Trzebicka, J. Sun, L. Liu, M.-S. Wang, M. H. Rümmeli, *Sci. China Mater.* **2022**, *65*, 2343; b) C. K. Chan, H. Peng, G. Liu, K. McIlwraith, X. F. Zhang, R. A. Huggins, Y. Cui, *Nat. Nanotechnol.* **2008**, *3*, 31.
- [21] J. Wang, J. Polleux, J. Lim, B. Dunn, *J. Phys. Chem. C* **2007**, *111*, 14925.
- [22] Y. Ren, L. Xiang, X. Yin, R. Xiao, P. Zuo, Y. Gao, G. Yin, C. Du, *Adv. Funct. Mater.* **2022**, *32*, 2110046.
- [23] S. K. Heiskanen, J. Kim, B. L. Lucht, *Joule* **2019**, *3*, 2322.
- [24] a) Y. Yu, C. Yang, Y. Jiang, J. Zhu, Y. Zhao, S. Liang, K. Wang, Y. Zhou, Y. Liu, J. Zhang, M. Jiang, *Small* **2023**, *19*, 2303779; b) Y. Ko, J. Bae, G. Chen, M. A. Baird, J. Yan, L. Klivansky, D.-M. Kim, S. E. Trask, M.-T. F. Rodrigues, G. M. Carroll, N. R. Neale, B. A. Helms, *ACS Energy Lett.* **2024**, *9*, 3448.

Manuscript received: March 12, 2025

Revised manuscript received: March 31, 2025

Version of record online: